Chinese Physics Letters

LETTER

Quantized Anomalous Hall Resistivity in Epitaxial $MnBi_2Te_4$ Thin Films on Ultrathin $Cr_2Ge_2Te_6$ Films

Cite as: Yang Chen *et al*. 2026 *Chin. Phys. Lett.* **43** 080701

DOI CSTR

Recommended Articles

Observation of Topological Hall Effect and Nernst Effect in the Canted Antiferromagnetic Phase of $MnBi_2Te_4$

Haiyang Yang *et al*.
Chin. Phys. Lett. **42**, 080706 (2025)

Effects of Thickness and Anisotropic Strain on Polarization Switching Properties of Sub-10nm Epitaxial $Hf_{0.5}Zr_{0.5}O_2$ Thin Films

Kuan Liu, Kai Liu, Xingchang Zhang, Jie Fang, Feng Jin, Wenbin Wu, Chao Ma, and Lingfei Wang
Chin. Phys. Lett. **41**, 117701 (2024)

Enhancement of Ising Superconductivity in $Pb_{1-x}Bi_x$ Ultrathin Films

Yitong Gu *et al*.
Chin. Phys. Lett. **42**, 057405 (2025)

Unveiling of Terahertz Emission from Ultrafast Demagnetization and the Anomalous Hall Effect in a Single Ferromagnetic Film

Zhiqiang Lan, Zhangshun Li, Haoran Xu, Fan Liu, Zuanming Jin, Yan Peng, and Yiming Zhu
Chin. Phys. Lett. **41**, (2024)

Ultrathin Limit on the Anisotropic Superconductivity of Single-Layered Cuprate Films

Feng Ran, Pan Chen, Dingyi Li, Peiyu Xiong, Zixin Fan, Haoming Ling, Yan Liang, and Jiandi Zhang
Chin. Phys. Lett. **41**, (2024)

A series journal of Chinese Physical Society distributed by IOP Publishing

Chinese Physics Letters

Chin. Phys. Lett. **43** 080701 (2026)

LETTER

DOI: 10.1088/0256-307X/43/8/080701
CSTR: 32039.14.0256-307X.43.8.080701

Quantized Anomalous Hall Resistivity in Epitaxial $MnBi_2Te_4$ Thin Films on Ultrathin $Cr_2Ge_2Te_6$ Films

Yang Chen(陈阳)[1,2,†], Pengfei Ji(纪蓬飞)[1,2,†], Tianchen Zhu(诸天晨)[1,2,†], Jianli Luan(栾建立)[1,2,†], Houyang Xia(夏厚阳)[1,2], Yitian Tong(仝一天)[1,2], Yunhe Bai(白云鹤)[1,2], Ruixuan Liu(刘瑞轩)[1,2], Xiyu Hong(洪熹宇)[1,2], Zhe Li(李哲)[6], Qi-Kun Xue(薛其坤)[1,2,3,4,5], Yang Feng(冯洋)[3], Ke He(何珂)[1,2,3,5,*], and Xiao Feng(冯硝)[1,2,5,*]

[1]State Key Laboratory of Low Dimensional Quantum Physics, Department of Physics, Tsinghua University, Beijing 100084, China
[2]Frontier Science Center for Quantum Information, Beijing 100084, China
[3]Beijing Academy of Quantum Information Sciences, Beijing 100193, China
[4]Southern University of Science and Technology, Shenzhen 518055, China
[5]Hefei National Laboratory, Hefei 230088, China
[6]Beijing National Laboratory for Condensed Matter Physics, and Institute of Physics, Chinese Academy of Sciences, Beijing 100190, China

[†]These authors contributed equally to this work
[*]Corresponding authors. Email: kehe@mail.tsinghua.edu.cn; xiaofeng@mail.tsinghua.edu.cn

$MnBi_2Te_4$ (MBT), as the first-discovered intrinsic magnetic topological insulator, has emerged as an attractive platform for realizing the high-temperature quantum anomalous Hall (QAH) effect. One approach to elevate the occurring temperature of the QAH effect in an MBT thin film is to introduce neighboring ferromagnetic insulator layers which may reinforce its magnetic order near the surface layers. In this work, we achieved high-quality heterostructures between MBT and ferromagnetic insulator $Cr_2Ge_2Te_6$ (CGT) thin films with molecular beam epitaxy. By investigating their transport properties at low temperatures, we found that a few-layer CGT buffer layer facilitates high-field quantized transport behavior in MBT films of 3-septuple-layer—the theoretical lower thickness limit of the QAH phase—whereas most early MBT samples, whether thin flakes or epitaxial thin films, become highly insulating at that thickness. These results demonstrate that few-layer CGT serves as an excellent magnetic proximity layer for MBT films, well keeping their intrinsic topological electronic structures and quantized transport properties. CGT/MBT heterostructures thus provide a viable route for exploring high-temperature QAH insulator as well as other novel topological phases in the future.

$MnBi_2Te_4$ (MBT) is the first intrinsic magnetic topological insulator and hosts a variety of topological quantum states in different geometry and spin configurations [1−6]. Since its discovery, MBT has attracted extensive attention due to its potential for realizing the high-temperature quantum anomalous Hall (QAH) effect. Notable transport phenomena, including the QAH state and axion insulator state, have been observed in mechanically exfoliated flakes derived from bulk single crystals [6−11]. Compared to exfoliated flakes, molecular beam epitaxy (MBE)-grown MBT films provide excellent scalability, reproducibility, and flexibility for multi-device fabrication and complex heterostructure integration. High-field quantized transport properties have been reported in MBT films grown on sapphire with in situ oxygen exposure and electrostatic gating [12].

However, such quantized transport behavior can only be achieved under high magnetic fields at ultralow temperatures, while zero-field quantization remains challenging [12−14]. Magnetic force microscopy measurements of MBE-grown MBT films revealed spatial magnetization inhomogeneity, which is likely attributed to intrinsic sample inhomogeneity, such as local strain variations or chemical disorders [15]. To address this issue, one feasible approach is to explore new substrates or interfaces that support the growth of MBT films with higher spatial uniformity. Another strategy is to introduce strong magnetic exchange coupling to establish a more uniform magnetic configuration in the topological surface states (TSS) of MBT. $Cr_2Ge_2Te_6$ (CGT) is a layered van der Waals ferromagnetic insulator with a bulk Curie temperature of approximately 61 K [16,17]. Theoretical calculations demonstrate that adjacent magnetic insulating layer, such as CGT, could have strong exchange coupling and electronic hybridization with MBT, thereby modifying the magnetic gap of the TSS and exhibiting great potential for realizing the QAH effect in ferromagnetic insulator (FMI)/topological insulator (TI) sandwich structures [18−22]. In this context, CGT serves as a suitable magnetic proximity layer for MBT heterostructures [22]. CGT thin films have been achieved by MBE and scotch tape method [18,23−28]. Although magnetic proximity effects were observed through transport measurements, the anomalous Hall resistivity was far from the quantized value [18,26,29−33].

In this study, we developed high-quality MBT/CGT heterostructures and investigated their electrical transport properties at ultralow temperatures. We found that a CGT buffer layer significantly improves the transport properties of MBT and facilitates high-field quantized transport behavior in 3-septuple-layer (3-SL) MBT, whereas thicker films exhibited a gradual deviation from quantization. These results demonstrate that CGT serves as an effective interfacial platform for enhancing the quantized transport properties of MBT thin films.

The MBT/CGT heterostructures were prepared with MBE on Si(111) substrates. A 2-layer (2-L) CGT film was first grown on the Si substrate, followed by the growth of MBT. After growth, the samples were annealed at the growth temperature for 30 minutes to improve the crystalline quality. The high crystalline quality of the heterostructure is evidenced by the reflection high-energy electron diffraction (RHEED) patterns which exhibit 7×7 reconstruction of Si(111) substrate and sharp streaky features after the growth of both CGT and MBT [Fig. 1(a)]. High-resolution high-angle annular dark-field (HAADF) scanning transmission electron microscopy (STEM) imaging further verifies atomically sharp interface between the 2-L CGT and MBT films [Fig. 1(b)]. The MBT film displays the characteristic septuple-layer structure. Angle-resolved photoelectron spectroscopy (ARPES) measurements on a 5-SL MBT/2-L CGT heterostructure reveal a clear Dirac-cone-shaped feature, which is the characteristic band structure of MBT and consistent with previous studies

Received 18 May 2026; accepted 23 June 2026; published 16 July 2026
© 2026 Chinese Physical Society and IOP Publishing Ltd. All rights, including for text and data mining, AI training, and similar technologies, are reserved.

Check for updates

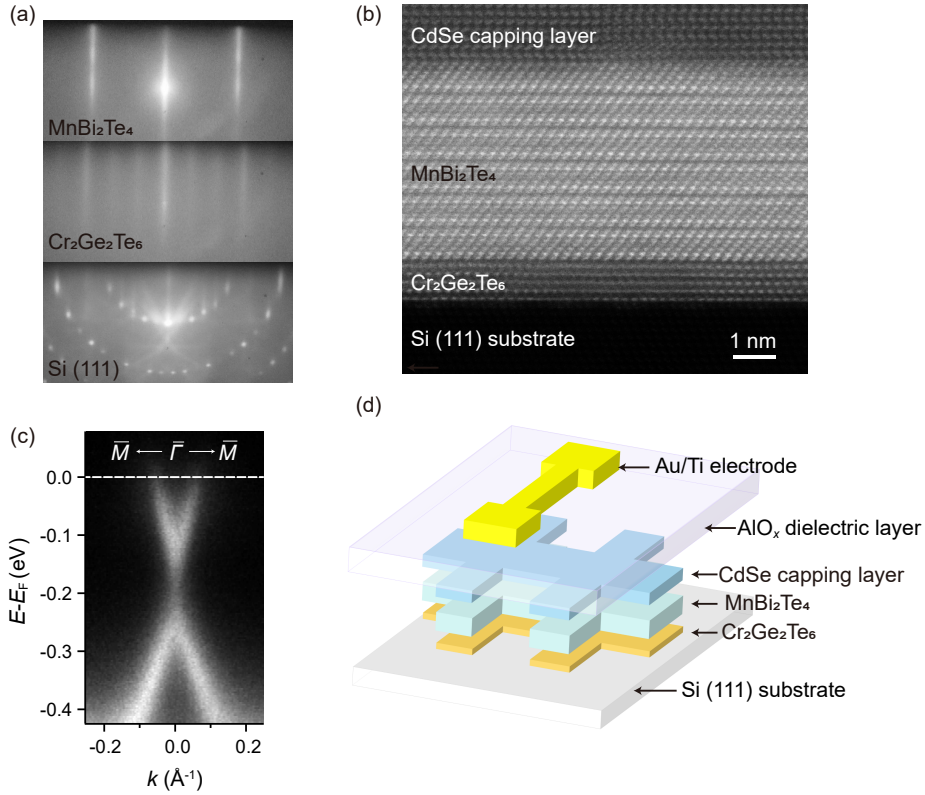

Fig. 1. Growth and structural characterization of the MBT/CGT heterostructure. (a) RHEED patterns of Si(111) substrate with 7×7 reconstruction, CGT film, and MBT film. (b) Cross-sectional HAADF-STEM image of the heterostructure. (c) ARPES spectrum of a 5-SL MBT/2-L CGT heterostructure grown on a conducting Si(111) substrate. (d) Schematic illustration of the Hall-bar device.

[Fig. 1(c)]. Atomic force microscopy (AFM) measurements reveal a uniform surface morphology with only occasional islands and depressions of 1-SL height [see Fig. S1(a) in the Supplementary Materials (SM)].

As-grown MBT films are typically n-type doped due to Bi_{Mn} antisite defects [34,35]. Effective and accurate carrier tuning is essential for the realization of quantized transport behavior. The samples were first exposed in situ to oxygen (5.4×10^{-3} mbar for 1.5 h) at room temperature as a coarse carrier-tuning method, which has previously been demonstrated to promote the quantized transport in MBT films grown on sapphire without degrading the film quality [12]. A 6-nm CdSe capping layer was subsequently deposited to protect the heterostructure against the ambient degradation. For electrical transport measurements, the films were patterned into Hall-bar devices (40 μm×80 μm) with Ar ion etching through a shadow mask. An AlO_x dielectric layer (~40 nm) and a top-gate electrode of (20 nm) Au/ (5 nm) Ti were subsequently fabricated by atomic layer deposition (ALD) and metal evaporation, respectively, enabling fine-tuning of the chemical potential, as illustrated schematically in Fig. 1(d).

Among different thicknesses of CGT and MBT, the 3-SL MBT/2-L CGT heterostructure exhibited well-quantized transport behavior under high magnetic fields. As shown in Figs. 2(a) and 2(b), the magnetic-field ($\mu_0 H$) dependences of the Hall (ρ_{yx}) and longitudinal (ρ_{xx}) resistivities were measured at the charge-neutral point (CNP) over a broad temperature range of 0.3 K–10.5 K. At 0.3 K, ρ_{yx} approaches the quantized value of h/e^2, while ρ_{xx} is strongly suppressed under high magnetic fields. In contrast, near zero field, ρ_{xx} becomes extremely large and ρ_{yx} exhibits strong fluctuations due to the low signal-to-noise ratio, indicating that the sample remains highly insulating. As the temperature increases, ρ_{yx} gradually deviates from h/e^2, and ρ_{xx} increases at high magnetic fields, indicating a progressive weakening of the quantized transport behavior. ρ_{xx} around zero field decreases with temperature, which is consistent with the insulating behavior.

Figure 2(c) displays the gate-voltage (V_g) dependences of ρ_{yx} and ρ_{xx} at 0.3 K and −9 T. ρ_{yx} approaches h/e^2 and develops a broad plateau, whereas ρ_{xx} is simultaneously reduced to ~0.45 h/e^2 near $V_g \approx$ 3.3 V. The remaining finite ρ_{xx} suggests that dissipative channels have not yet been fully eliminated at 0.3 K, although the quantization of ρ_{yx} is well developed. The temperature evolution of ρ_{yx} and ρ_{xx} at V_g = 3.3 V is summarized in Figs. 2(d) and 2(e), respectively. At −9 T, ρ_{yx} decreases monotonically from h/e^2 at 0.3 K to 0.67 h/e^2 at 10 K, while ρ_{xx} increases and approaches ~0.9 h/e^2. These opposite temperature dependences under high fields further indicate that the system enters a well-developed high-field quantized transport regime at low temperatures. In contrast, the zero-field ρ_{xx} decreases rapidly with increasing temperature, which is consistent with the gradual weakening of the highly insulating state. Similar high-field quantization and temperature evolution trends were also observed in 4-SL MBT grown on 2-L CGT, as shown in Fig. S2 of the SM.

The thickness-dependent transport properties of MBT films grown on 2-L CGT are presented in Fig. 3. Figure 3(a) shows the temperature dependences of ρ_{xx} measured at zero magnetic field. All samples exhibit insulating behavior. Meanwhile, the overall magnitude of ρ_{xx} decreases with increasing MBT thickness, indicating enhanced bulk contribution in thicker films. The magnetic-field- and gate-voltage-dependent transport properties measured at 2 K are shown in Figs. 3(b)–3(d). The 2-SL MBT exhibited strongly insulating behavior. Even under high magnetic fields, ρ_{xx} exceeds 20 h/e^2, whereas ρ_{yx} remains far below h/e^2, indicating the absence of topological edge states. The insulating behavior is primarily attributed to the strong hybridization between the top and bottom surface states in the ultrathin limit [3,36]. In contrast, as the MBT thickness increases to 3-SL and 4-SL, ρ_{yx} approaches h/e^2 and the maximum of ρ_{yx} coincides with the minimum of ρ_{xx} as a function of gate voltage, which is the characteristic signature of edge-state-dominated transport behavior. However, as the MBT thickness further increases to 5-SL and beyond, ρ_{yx} gradually deviates from the ideal quantized regime accompanied by a corresponding decrease in ρ_{xx}. The progressive reduction of ρ_{yx} indicates that the residual dissipative conduction channels become dominant.

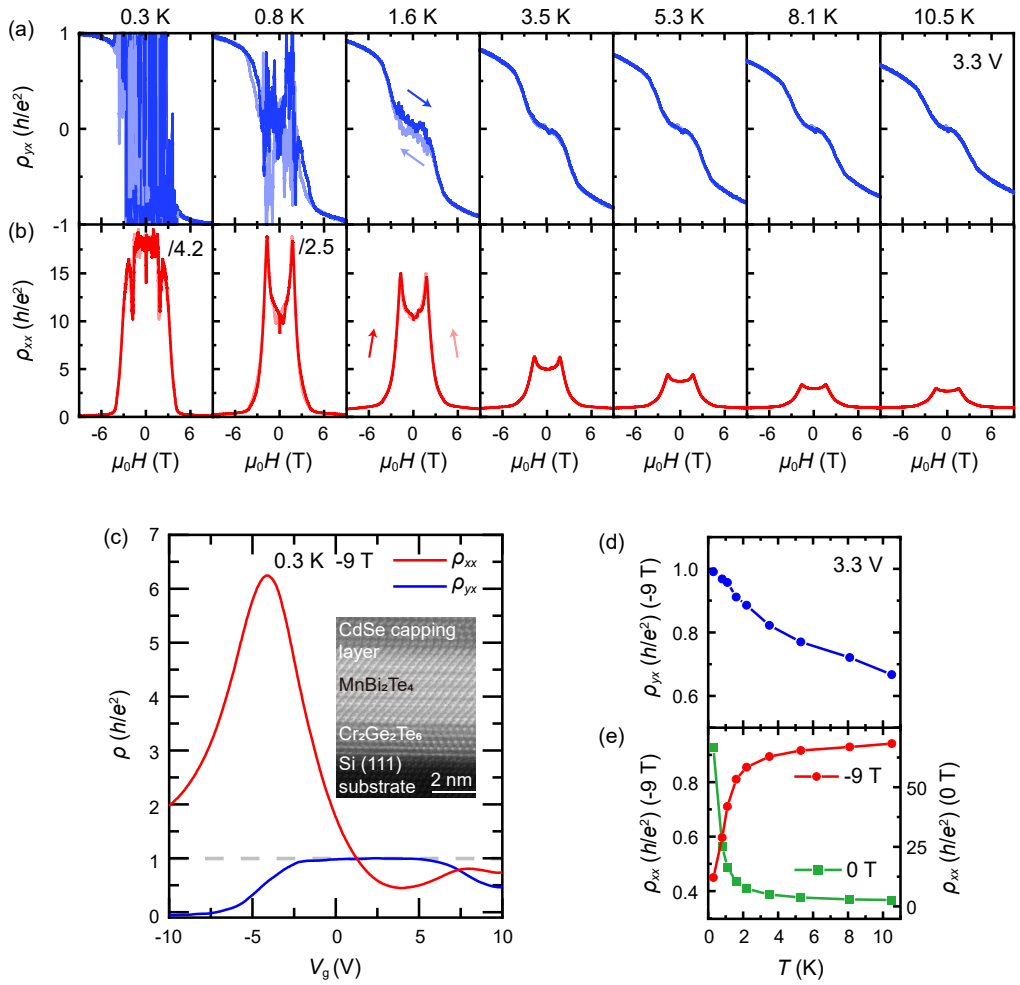

Fig. 2. Quantized transport properties of 3-SL MBT/2-L CGT heterostructure. (a) and (b) $\mu_0 H$ dependences of ρ_{yx} and ρ_{xx} measured at $V_g = 3.3$ V from 0.3 to 10.5 K, respectively. (c) V_g dependences of ρ_{xx} and ρ_{yx} measured at 0.3 K and −9 T. Inset: STEM image of the device. (d) Temperature dependence of ρ_{yx} measured at −9 T and $V_g = 3.3$ V. (e) Temperature dependence of ρ_{xx} measured at $V_g = 3.3$ V, where the left axis is ρ_{xx} at −9 T and the right axis is ρ_{xx} at 0 T.

Collectively, CGT provides a high-quality interface for MBT thin films, enabling the realization of quantized transport behavior in MBT/CGT heterostructures.

To realize the QAH effect, FMI/TI/FMI sandwich structures are more favorable. The symmetric 2-L CGT/3-SL MBT/2-L CGT sandwich structures were prepared on Si(111) substrate under growth conditions identical to those of the MBT/CGT heterostructure, except that no post-growth annealing was performed on the top CGT layer to minimize additional elemental diffusion across the interface.

The schematic illustration of the sandwich structure and the STEM image are shown in Figs. 4(a) and 4(b), respectively. The STEM image directly resolves the CGT/MBT/CGT structure, with the middle MBT layer sandwiched between the top and bottom CGT layers, and all interfaces remain well-defined and distinguishable. Figure 4(c) depicts the temperature dependence of ρ_{xx}, which exhibits typical insulating behavior with a Néel temperature of ~19.7 K. The V_g dependences of ρ_{xx} and ρ_{yx} measured at 2 K and −8 T are displayed in Fig. 4(d). Only a weak variation in ρ_{xx} was observed, whereas ρ_{yx} exhibited nearly no gate-dependence behavior and remained far below h/e^2. This observation suggests that the carrier density in the middle-MBT layer cannot be effectively modulated by the top gate alone.

The magnetic-field dependences of ρ_{xx} and ρ_{yx} are displayed in Figs. 4(e) and 4(f), respectively. The values of ρ_{xx} at zero and high magnetic fields are comparable, both on the order of 2 h/e^2. The high-field ρ_{xx} is significantly larger than that of the MBT/CGT heterostructure. At high magnetic fields, ρ_{yx} is approximately 0.25 h/e^2, which is far below the quantized value. A distinct anomalous Hall hysteresis is observed near zero magnetic field, but with a reversed sign compared to MBT films, which will be briefly discussed later. These results indicate that, in contrast to the MBT/CGT heterostructure in Fig. 2, the sandwich sample is far from the quantized transport regime. The absence of quantized transport result can be attributed to lack of an efficient carrier tuning method, as the chemical potential of the middle MBT layer cannot be efficiently driven toward the CNP. Consequently, residual electron carriers in MBT layer cannot be sufficiently compensated, leading to substantial dissipative bulk conduction. Usually, a post-growth annealing treatment is applied after the growth of CGT to enhance the crystalline quality [25]. However, no post-growth annealing was conducted on the top CGT layer to avoid potential Cr diffusion, which could introduce interface defect states acting as charge traps, shielding, or localizing the carriers injected by the gate electric field. This issue requires further investigation and optimization in future work.

Although quantized anomalous Hall resistivity has been observed in 5-SL MBT thin films grown on sapphire substrates, 3-SL MBT remains strongly insulating even under high magnetic fields, and 4-SL MBT failed to achieve quantized Hall resistivity even at 30 mK [12]. In contrast, both 3-SL and 4-SL MBT films grown on 2-L CGT exhibit quantized transport behavior. This difference indicates that the CGT interface plays a critical role in enabling high-field quantized transport in ultrathin MBT films.

Two key factors are proposed to induce these distinct transport behaviors. First, CGT buffer layer may provide a higher-quality interface for MBT growth, thereby enhancing the crystalline order which is essential for robust quantized transport. Second, the hybridization

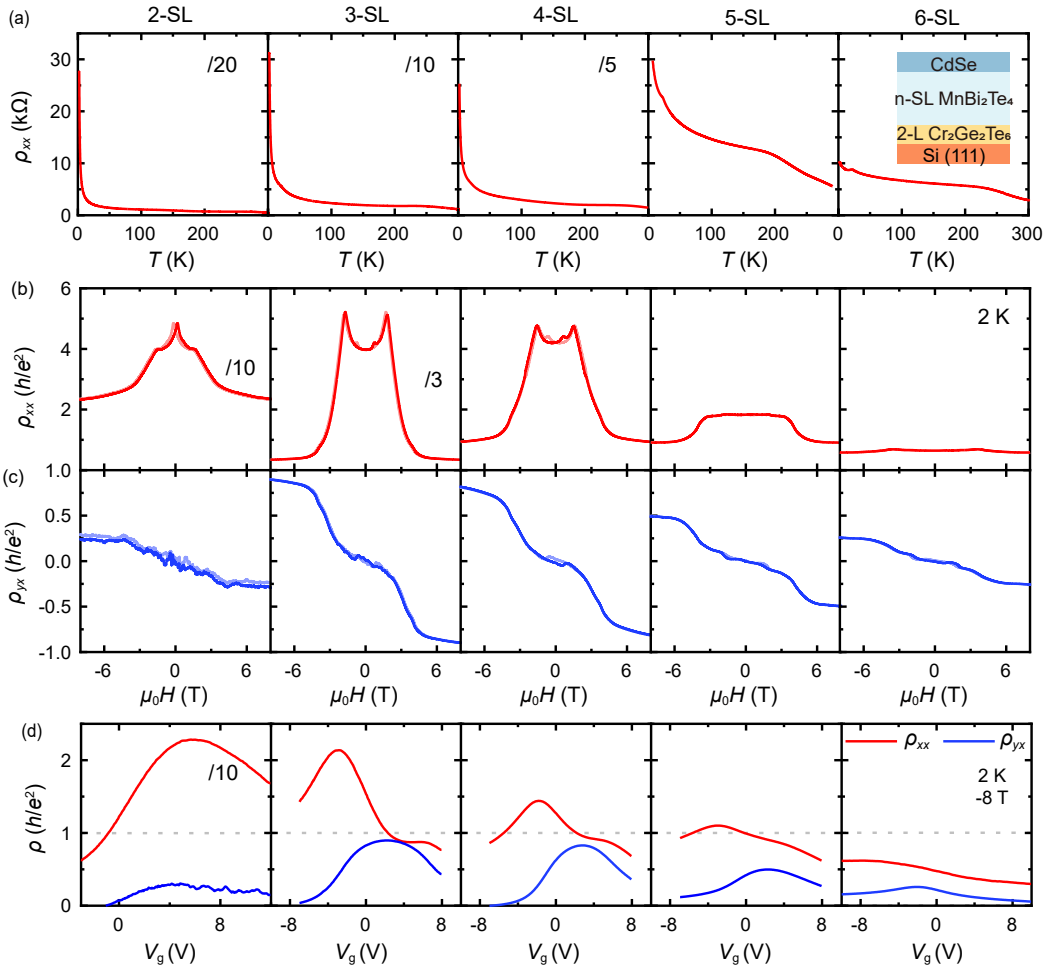

Fig. 3. Thickness-dependent transport properties of MBT films grown on 2-L CGT. (a) Temperature dependences of ρ_{xx} measured at zero magnetic field. (b) and (c) $\mu_0 H$ dependences of ρ_{xx} and ρ_{yx}, respectively, measured at 2 K near the CNP. Inset: the schematic illustration of the device. (d) V_g dependences of ρ_{xx} and ρ_{yx} measured at 2 K and −8 T.

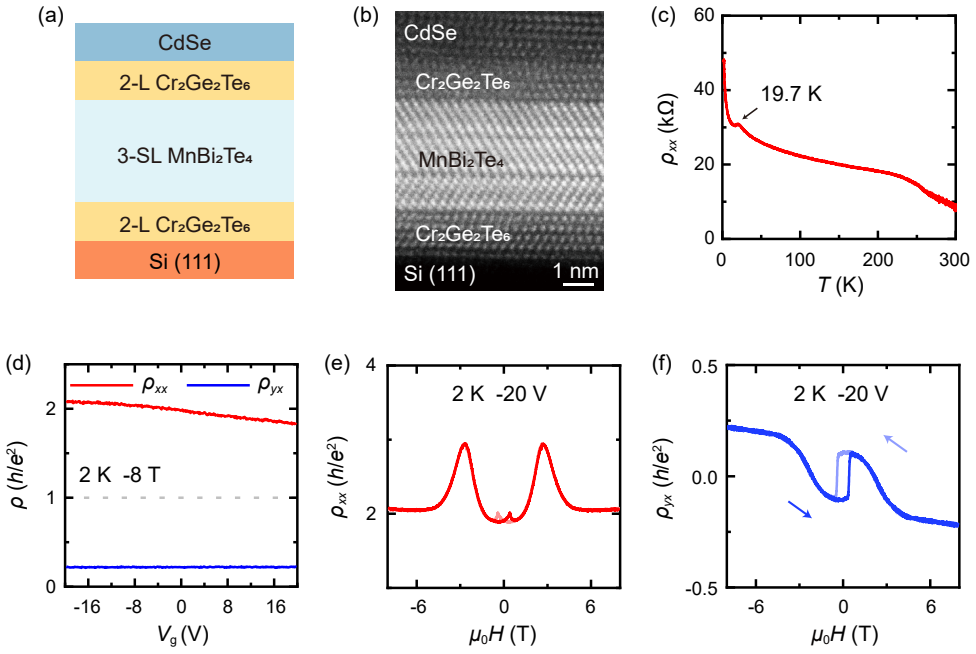

Fig. 4. Characterization of the CGT/MBT/CGT sandwich structure. (a) Schematic illustration of the sample. (b) Cross-sectional STEM image of the CGT/MBT/CGT sandwich structure. (c) Temperature dependence of ρ_{xx}. (d) V_g dependences of ρ_{xx} and ρ_{yx} measured at 2 K and −8 T. (e) and (f) $\mu_0 H$ dependences of ρ_{xx} and ρ_{yx}, respectively, measured at 2 K with $V_g = -20$ V.

between the top and bottom TSSs may be different in MBT films on CGT buffer layer. In MBT films grown on sapphire, the highly insulating 3-SL film suggests strong hybridization between the TSSs of two surfaces in the ultrathin limit. Most early MBT samples, either thin flakes or epitaxial thin films, also become highly insulating below 5-SL. In contrast, the observation of quantized transport in 3-SL MBT on CGT indicates that the TSSs from the two surfaces remain effectively decoupled. It is worth noting that 3-SL is the theoretical lower thickness limit of the QAH phase in $MnBi_2Te_4$ [1−5]. The insulating behavior in early $MnBi_2Te_4$ samples below 5-SL has been attributed to deterioration of surface layers or the redistribution of the TSSs into the bulk by defects [37]. The quantized transport in 3-SL MBT films on CGT suggests that the TSSs in these samples are closer to that of the pristine MBT in theory. First-principle calculations on CGT/Bi_2Te_3/CGT and CGT/Sb_2Te_3/CGT sandwiches have shown that a significant portion of the TSS wave function is redistributed in the outmost CGT layers [22]. Probably, the redistribution effect of the MBT TSSs by CGT layers (towards the surface) and by defects (towards the bulk) is largely cancelled out by each other, leading to a situation closer to a pristine MBT film.

However, 5-SL and thicker MBT films on 2-L CGT layer obviously deviate from the quantized regime, different from MBT films on sapphire substrates. As mentioned above, the carrier density of MBT thin films can be tuned by controlled oxygen exposure, top-gate electric fields, and interfacial doping from the underlying substrate or adjacent layers. For MBT films grown on sapphire, the chemical potential near the top surface is tuned by oxygen exposure (1×10^{-3} mbar for 1 h), while that near the bottom surface is tuned by the sapphire substrate [12]. We found that MBT films grown on 2-L CGT require a higher oxygen exposure (5.4×10^{-3} mbar for 1.5 h) to approach charge neutrality. It suggests that MBT films on CGT buffer layer possess a higher residual electron density compared to those on sapphire. Therefore, only for thinner MBT films, such as 3-SL, oxygen exposure and top-gate tuning can drive the samples near charge neutrality and thus into the QAH phase.

The transport behavior of the CGT/MBT/CGT sandwich structure can be understood within the same framework. In this structure, the top CGT layer screens the external top-gate electric field and blocks efficient oxygen exposure. Consequently, neither side of the MBT film can be tuned to charge neutrality.

In contrast to the high-field quantization behavior, thin MBT/CGT heterostructures remain strongly insulating at zero magnetic field. Moreover, the Hall resistivity near zero field is strongly suppressed and exhibits an anomalous Hall response with a sign opposite to that typically observed in intrinsic MBT films, as illustrated in the heterostructure sample in Fig. 2(a) above 3.5 K and the sandwich sample in Fig. 4(f) (see Fig. S6 of the SM for details). The anomalous Hall effect with a hysteresis chirality opposite to that of intrinsic MBT films has been reported in TIs adjacent to CGT [25,29,30]. Additionally, the magnetic gap induced by Cr and Mn in CGT/3-SL MBT/CGT sandwich structures was predicted to exhibit opposite chirality [22]. These observations suggest that the zero-field Hall signal in MBT/CGT heterostructures may result from cancellation of the anomalous Hall contributions from MBT and from CGT. In the CGT/MBT/CGT sandwich structure, the proximity-induced Hall response from CGT dominates at zero magnetic field, leading to a clear anomalous Hall hysteresis with a reversed sign [Fig. 4(f)]. The microscopic origin of the complex proximity-induced anomalous Hall response from the CGT layer and the possible interfacial exchange coupling requires further systematic investigations.

Conclusions

In summary, high-quality MBT/CGT heterostructures were successfully grown by MBE, with quantized transport behavior observed. On the optimized 2-L CGT buffer layer, 3-SL MBT film exhibits a quantized ρ_{yx} plateau and strongly suppressed ρ_{xx}, demonstrating the Chern insulator phase. With increasing film thickness, ρ_{yx} progressively deviates from the ideal quantized regime, which can be attributed to the relatively weak p-type compensation provided by CGT and the resulting residual electrons near the MBT/CGT interface. CGT/MBT/CGT sandwich structures were also prepared. However, the top CGT layer prevents efficient carrier-density tuning, resulting in the absence of quantization. These results indicate that few-layer CGT films can support MBT films with quantized transport properties. As long as the carrier-tuning issue of MBT films is solved, one may explore higher temperature QAH insulator and other novel topological phases by building various heterostructures between few-layer MBT and CGT films.

Acknowledgments

This work was supported by the National Natural Science Foundation of China (Grant Nos. 92565302 and 12374184) and the Quantum Science and Technology-National Science and Technology Major Project (Grant No. 2021ZD0302502).

References

[1] Li J H, Li Y, Du S Q *et al*. 2019 *Sci. Adv.* **5** eaaw5685
[2] Zhang D Q, Shi M J, Zhu T S, Xing D Y, Zhang H J, and Wang J 2019 *Phys. Rev. Lett.* **122** 206401
[3] Otrokov M M, Rusinov I P, Blanco-Rey M *et al*. 2019 *Phys. Rev. Lett.* **122** 107202
[4] Otrokov M M, Klimovskikh I I, Bentmann H *et al*. 2019 *Nature* **576** 416
[5] Gong Y, Guo J W, Li J H *et al*. 2019 *Chin. Phys. Lett.* **36** 076801
[6] Deng Y J, Yu Y J, Shi M Z *et al*. 2020 *Science* **367** 895
[7] Liu C, Wang Y C, Li H *et al*. 2020 *Nat. Mater.* **19** 522
[8] Ge J, Liu Y Z, Li J H *et al*. 2020 *Natl. Sci. Rev.* **7** 1280
[9] Zhang C S, Lu X F, Wang N Z *et al*. 2025 *Nat. Commun.* **16** 5587
[10] Wang Y Q, Fu B H, Wang Y C *et al*. 2025 *Nat. Commun.* **16** 1727
[11] Lian Z C, Wang Y C, Wang Y Q *et al*. 2025 *Nature* **641** 70
[12] Bai Y H, Li Y Z, Luan J L *et al*. 2024 *Natl. Sci. Rev.* **11** nwad189
[13] Li Q L, Mo S K, and Edmonds M T 2024 *Nanoscale* **16** 14247
[14] Li Y Z, Bai Y H, Feng Y *et al*. 2024 arXiv: 2401.11450 [cond-mat.mes-hall]
[15] Shi Y, Bai Y H, Li Y Z *et al*. 2024 *Phys. Rev. Mater.* **8** 124202
[16] Carteaux V, Brunet D, Ouvrard G, and Andre G 1995 *J. Phys.: Condens. Matter* **7** 69
[17] Zhang X, Zhao Y L, Song Q, Jia S, Shi J, and Han W 2016 *Jpn. J. Appl. Phys.* **55** 033001
[18] Fang J Z, Cui H N, Wang S *et al*. 2023 *Phys. Rev. B* **107** L041107
[19] Fu H X, Liu C X, and Yan B H 2020 *Sci. Adv.* **6** eaaz0948
[20] Nogues J and Schuller I K 1999 *J. Magn. Magn. Mater.* **192** 203
[21] Wang F, Xiao D, Yuan W *et al*. 2019 *Nano Lett.* **19** 2945
[22] Li Z, Xue F, Tang X Y, Hong X Y, Chen Y, Feng X, and He K 2025 *Phys. Rev. B* **111** 075106
[23] Gong C, Li L, Li Z L *et al*. 2017 *Nature* **546** 265
[24] Chau T K, Hong S J, Kang H, and Suh D 2022 *npj Quantum Mater.* **7** 27
[25] Ji P F, Liu R X, Zhu T C *et al*. 2026 *Adv. Mater.* e72994
[26] Mogi M, Tsukazaki A, Kaneko Y, Yoshimi R, Takahashi K S, Kawasaki M, and Tokura Y 2018 *APL Mater.* **6** 091104
[27] Xing W Y, Chen Y Y, Odenthal P M *et al*. 2017 *2D Mater.* **4** 024009
[28] Wang Z, Zhang T Y, Ding M *et al*. 2018 *Nat. Nanotechnol.* **13** 554
[29] Mogi M, Nakajima T, Ukleev V *et al*. 2019 *Phys. Rev. Lett.* **123** 016804
[30] Mogi M, Yasuda K, Fujimura R *et al*. 2021 *Nat. Commun.* **12** 1404
[31] Gupta V, Jain R, Ren Y F *et al*. 2022 *Nano Lett.* **22** 7166
[32] Llacsahuanga Allcca A E, Pan X C, Miotkowski I, Tanigaki K, and Chen Y P 2022 *Nano Lett.* **22** 8130
[33] Nagata K, Matsushita S Y, Pan X C, Huynh K K, and Tanigaki K 2021 *Phys. Rev. Mater.* **5** 024208
[34] Huang Z, Du M H, Yan J, and Wu W 2020 *Phys. Rev. Mater.* **4** 121202
[35] Zeugner A, Nietschke F, Wolter A U B *et al*. 2019 *Chem. Mater.* **31** 2795
[36] Xu R Z, Bai Y H, Zhou J S *et al*. 2022 *Nano Lett.* **22** 6320
[37] Tan H X and Yan B H 2023 *Phys. Rev. Lett.* **130** 126702